Hindawi
Journal of Chemistry
Volume 2023, Article ID 2245685, 17 pages
https://doi.org/10.1155/2023/2245685

Research Article

Green Synthesis by Microwave Irradiation of TiO_2 Using *Cinnamomum verum* and the Application in Photocatalysis

Dante E. González-Anota,[1] **Silvia P. Paredes-Carrera**,[1] **Rosa M. Pérez-Gutierrez**,[2] **Brandon Arciniega-Caballero**,[1] **Raul Borja-Urby**,[3] **Jesús C. Sánchez-Ochoa**,[1] **and Elizabeth Rojas-García**[4]

[1]*Laboratorio de Nanomateriales Sustentables, Escuela Superior de Ingeniería Química e Industrias Extractivas (ESIQIE), Instituto Politécnico Nacional (IPN), Unidad Profesional Adolfo López Mateos, Av. Instituto Politécnico Nacional S/N, Ciudad de México, CP 07708, Mexico*
[2]*Laboratorio de Productos Naturales, Escuela Superior de Ingeniería Química e Industrias Extractivas (ESIQIE), Instituto Politécnico Nacional (IPN), Unidad Profesional Adolfo López Mateos, Av. Instituto Politécnico Nacional S/N, Ciudad de México, CP 07708, Mexico*
[3]*Centro de Nanociencias y Micro y Nanotecnologías (CNMN), Instituto Politécnico Nacional (IPN), Unidad Profesional Adolfo López Mateos, Av. Luis Enbrique Erro S/N, Ciudad de México, CP 07708, Mexico*
[4]*Area de Ingeniería Química, Departamento de Ingeniería de Procesos e Hidráulica, Universidad Autónoma Metropolitana (UAM), Campus Iztapalapa, Ciudad de México, CP 09310, Mexico*

Correspondence should be addressed to Silvia P. Paredes-Carrera; silviappcar@gmail.com

Received 14 October 2022; Revised 21 November 2022; Accepted 3 April 2023; Published 12 May 2023

Academic Editor: B. R. Ramesh Bapu

The extraction process of bioactives from the aqueous extract of cinnamon (*Cinnamomum verum*) was optimized using the Design Expert 11 program and analysis of variance (ANOVA) by considering the following parameters: cinnamon weight (g), power (W), and time (s) of microwave irradiation. The optimal conditions are cinnamon weight of 4.5 grams, time of 600 seconds, and power of 150 watts of microwave irradiation. With *Cinnamomum verum* extract under optimal conditions and titanium (IV) tetrachloride as a precursor, TiO_2 nanostructures were synthesized using the sol-gel method assisted by microwave irradiation in the crystallization stage with a power and irradiation time of 150 W and 600 sec, respectively. Similarly, a sample without extract was synthesized under the same conditions. The following techniques characterized the materials: X-ray diffraction (XRD), Fourier transform infrared (FTIR) spectroscopy, UV-vis diffuse reflectance, Raman spectrometry, and high-resolution transmission electron microscopy (HRTEM). It was feasible to obtain nanocrystalline solids of TiO_2 anatase phase with and without cinnamon extract; the particle size and the crystallinity were influenced by the bioactive agents during the synthesis (aqueous extract of *Cinnamomum verum*) and the synthesis method (microwave irradiation); a smaller crystal size, a smaller particle size, a higher crystalline order, and a lower band gap were achieved for the material synthesized with cinnamon extract compared to the material synthesized without extract and other methods. The synthesized materials were evaluated in the photodegradation of methyl orange (as a model of photodegradation), employing as reference parameters the commercial TiO_2 brand Sigma-Aldrich phase anatase and the photolysis of the system. The amount of dye adsorbed in the tested materials was quantified, finding an equilibrium time of 15 min, where the TiO_2 synthesized with *Cinnamomum verum* extract was the material that most adsorbed methyl orange at 7.5%. In the case of photodegradation, the TiO_2 synthesized with cinnamon extract apparently promoted the total mineralization of methyl orange in 40 minutes of reaction, making it the best material of those evaluated in the photodegradation. In all cases, the degradation models were adjusted to a first-order kinetic model, where it was confirmed that the highest reaction rate corresponded to TiO_2 synthesized with *Cinnamomum verum*.

1. Introduction

The generation of nanomaterials through green synthesis uses low-cost sustainable methodologies with low or zero emission of waste and toxic by-products [1, 2] as an alternative to existing synthesis methods such as coprecipitation, solvothermal, and the sol-gel method, among others, that require a high energy expenditure and purification and generate toxic by-products and waste for the environment [3].

In green synthesis, natural sources such as microorganisms (bacteria, fungi, and yeasts), extracts of plants (flowers, stems, and leaves), or products of metabolism or parts of them (enzymes) are used [4, 5]. Natural extracts contain bioactive compounds present in plants, such as alkaloids, polyphenols, terpenoids, antioxidants, sugars, flavonoids, organic acids, and quinones, together with low molecular weight proteins [6] which can be used in the reduction of precursor agents for the synthesis of nanomaterials [4, 7] because they act as electron donors [8], stabilizers, and capping agents [9–11]. Coating agents prevent coagulation and spontaneous flocculation of the precursors and intermediate products during the synthesis processes through electrostatic interaction [12].

A viable biological material for the green synthesis of nanomaterials is cinnamon (*Cinnamomum verum*) due to its high content of bioactive compounds such as aldehydes, alcohols, esters, acids, monoterpenes, diterpenes, sesquiterpenes, benzopyrenes, hydrocarbons, flavonoids (procyanidin dimers type A and B), and phenolic compounds (eugenol and pyrogallol). Previous studies have shown that the aqueous extract of *Cinnamomum veru*m has high antioxidant activity [13, 14], which suggests its application in the synthesis of nanomaterials as an effective reducing agent for metallic particles and promoting chemical processes such as hydrolysis [15]; in addition, no reported applications for the synthesis of nanomaterials were found for this compound.

The nanomaterial employed in this work was titanium dioxide (TiO_2), with high photocatalytic activity (>50–80% in 2 H) [16, 17] and can be found in three crystalline structures: anatase, rutile, and brookite [18]. The anatase phase is the one with the highest photoactivity [19]. However, although TiO_2 is an excellent photocatalytic material, it also has some drawbacks since it has a limited absorption in the visible spectrum with a band gap of 3.2 eV [20], mainly absorbing UV radiation, with a high recombination rate of electron-hole pairs and presenting photo corrosion which decreases its photocatalytic efficiency. For this reason, various works [21–23] have sought to generate a change in the band pap, morphology, texture, and/or particle size [20, 24]. This is through doping (with noble metals such as silver and gold), coupling it to other semiconductors and/or materials such as graphene (composites and hybrid materials), with morphosynthesis (polymeric templates), and/or obtaining with different synthesis methodologies and precursors [25, 26]. This is where microwave-assisted green synthesis provides a viable and novel technology.

Microwave irradiation has been implemented in the search for methodologies that represent a lower energy expenditure and allows the manipulation of properties such as the texture and morphology of nanoparticles [27]. Microwaves are a type of electromagnetic radiation between 0.3 and 300 GHz; the heating mechanism involves two main processes: dipolar polarization and ionic conduction. Irradiation of a sample with microwaves results in the alignment of the dipoles or ions in the electric field. Because electromagnetic radiation produces an oscillating field, the dipoles or ions continually try to realign themselves in the electric field. Depending on the oscillation phenomena in relation to the frequency of the irradiation, different amounts of heat are produced through molecular friction and dielectric loss [28, 29]; this superheat allows a fast reaction speed, reproducibility, and control of the morphology and texture depending on the parameters of power and irradiation time [28, 30], which makes it a suitable irradiation source both for the extraction of bioactive compounds and for the synthesis of nanomaterials [30–32].

Methyl orange was used as a photodegradation model for the synthesized materials [33, 34], belonging to the azo dyes, and these constitute between 60 and 70% of the dyes used in the industry, being one of the most important contaminants that reproduce in the environment [35–37]. It is worth mentioning that the objective of this research is focused on the properties of TiO_2 synthesized by green synthesis by microwave irradiation of TiO_2 using *Cinnamomum verum* and its potential application, constituting a starting point for future work. The quantification of the percentage of methyl orange degradation was evaluated by UV-vis spectroscopy (467 nm).

On the other hand, the optimization of the aqueous extract of *Cinnamomun verum* was carried out using the Box–Behnken Design (BBD) model, which is one of the methods for predicting response surface methodologies (RSMs). This model has its origin from the graphic perspective and an adjustment through empirical models. The response surface methodology (RSM), introduced by George E. P. Box and K. B. Wilson in the early 1950s, consists of the collection of statistical and mathematical techniques useful for modeling and analyzing experimental data, which determine the effects and response of quantitative variables to identify the optimal point. The advantage is the decrease in the number of experiments to evaluate their independent variables, and the disadvantage is the inability to provide a global optimal point. The RSM largely uses the BBD response surface, which is suitable for fitting quadratic and cubic models and is feasible to investigate and optimize variables in the experimental space with the fewest number of experiments without being an expert in statistics. The central composite design (CCD) is based on the same criteria as BBD; however, the main difference between them is the number of star points or center points in the experimental space, which gives CCD more points and, therefore, more experiments. Compared to the "one-variable-at-a-time" approach and the full factorial design, the BBD has more advantages due to the reduced number of experiments [38–46].

In this work, we sought to obtain photocatalytic nanomaterials such as TiO_2 via green synthesis by the sol-gel method assisted with microwave irradiation of the TiO_2 type through the use of bioactive compounds from the aqueous extract of *Cinnamomum verum,* which were optimized using the RSM statistical technique, with the premise of obtaining efficient and economically sustainable nanomaterials that improve the photocatalytic processes.

2. Experimental

2.1. Chemicals. The reagents used for the preparation of the precursor solutions for the extraction of bioactives from cinnamon and TiO_2 synthesis were as follows: $TiCl_4$Sigma-Aldrich 99.9%, $C_{14}H_{14}N_3O_3SNa$ Sigma-Aldrich 99.9%, C_2H_5OH Sigma-Aldrich 98%, TiO_2Sigma-Aldrich 99.5%, and Caledon brand bidistilled, tridistilled, and deionized water.

2.2. Cinnamomum verum Aqueous Extract Optimization. Cinnamomum verum aqueous extract optimization by microwave irradiation was performed with the use of Design Expert software (Version 8.0.6, Stat-Ease Inc., Minneapolis, MN, USA). It employs the BBD as an algorithm, which is one of the methods for predicting response surface methodologies (RSMs) to examine the relationship between one or more response variables and a set of quantitative experimental parameters. The optimization was made using three independent variables and one response variable, with 17 runs to optimize the extraction conditions of bioactive (Table 1). Aqueous extracts of *Cinnamomum verum* were obtained in an SBL CW-2000A microwave reactor. The three independent variables were as follows: the weight of *Cinnamomum verum* (1.5, 3.0, and 4.5 g) with deionized water, microwave irradiation time (300, 600, and 900 s), and microwave irradiation power (150, 250, and 350 W); the response variable was the weight of the *Cinnamomum verum* extract. Regression analysis was made according to the experimental data, and the second-order polynomial model (equation (1)) was fitted to express the amount of extract obtained through the **AN**alysis **O**f **VA**riance (ANOVA) [47].

$$Y = a_0 + \sum_{i=1}^{3} a_i X_i + \sum_{i=1}^{3} a_{ii} X_i^2 + \sum_{i \neq J=1}^{3} a_{ij} X_i X_j, \qquad (1)$$

where Y is the amount of *Cinnamomum verum* extract, a_0 is the intersection (constant), $?_1X_1$ to $?_3X_3$ are linear coefficients, $a_{11}X_1^2$ to $a_{33}X_3^2$ are quadratic coefficients and interaction coefficients, X_1 is the weight of the *Cinnamomum verum* (g), X_2 is microwave irradiation power (W) y, and X_3 is the microwave irradiation time (s).

2.3. Green Synthesis of TiO_2 Nanoparticles by the Sol-Gel Method Assisted by Microwave Irradiation and Cinnamomum verum Extract as Reductant. In the synthesis of TiO_2 nanoparticles (a code **C-TiO_2** was assigned) using the sol-gel method assisted by microwave irradiation, 100 ml of *Cinnamomum verum* extract (prepared according to optimal results) was added to a flanged reactor, and the equivalent of 5% $TiCl_4$ was added dropwise, keeping the system under constant agitation for 40 minutes in a cryogenic bath at 4°C. Finally, the mixture was introduced into the SBL CW-2000A microwave reactor and irradiated for 10 minutes at 150 W. Washes were performed by centrifugation with a 1: 1 ethanol-water mixture at 15 000 rpm at room temperature for 15 minutes. The precipitate was dried in a convection oven for 5 hours at 70°C, and the resulting material was calcined for 4 hours at 450°C with a heating ramp of 30 minutes at $10°C \cdot min^{-1}$. The procedure was repeated without extract, and the code **CO-TiO_2** was assigned to this sample. It is worth mentioning that in the evaluation, Sigma-Aldrich brand TiO_2 was used as a reference, which was identified as **A-TiO_2**.

2.4. Characterization of the Samples. The synthesized compounds were characterized by X-ray diffraction (XRD), Fourier transform infrared spectroscopy (FTIR), UV-vis diffuse reflectance spectroscopy (UV-vis), Raman spectroscopy, and High-resolution transmission electron microscopy (HRTEM). The XRD spectra were obtained on a PANalytical model X'Pert PRO diffractometer for thin films or crystalline coatings ($\lambda = 1541$ Å), and the infrared spectra were obtained on a Nicolet Magna-IR 550 spectrometer in a range of 4000 – 650 cm. UV-vis spectra were obtained via a Cary 100 UV-vis spectrophotometer, with an integrating sphere (Labsphere DRA-CA-30) and was operated over a wavelength interval between 200 and 800 nm. Raman spectra were recorded at ambient temperature on a Raman Thermo Nicolet Almaga between 100 cm^{-1} and 1000 cm^{-1} with an exposure time of 1 s; the emission wavelength was 532 nm, and a nominal power of 25 mW was applied with a Nd: YVO4 laser. HRTEM and BFTEM micrograms were obtained in a transmission electron microscope JEOL brand JEM-ARM200CF model at 200 kV.

2.5. Evaluation of the Adsorption-Photodegradation of Methyl Orange

2.5.1. Adsorption of Methyl Orange. The materials were left in the dark in contact with the 3 ppm solution of methyl orange and found that the equilibrium time was 15 min. The adsorption of methyl orange was quantified in a Perkin Elmer brand UV-vis Lambda XLS spectrophotometer at a wavelength of 467 nm. After the adsorption, the materials were subjected to the photodegradation process.

2.5.2. Photodegradation of Methyl Orange. The process was carried out in 15 ml vials in triplicate for each point. 10 ml of methyl orange at 3 ppm and 0.1 g of C-TiO_2 were added to each vial; the resulting suspensions were subjected to UV light irradiation in a Luz Chem brand photoreactor equipped with 2 Philips 125 W UV lamps and an agitation system. Every 10 minutes, 5 ml aliquots were taken in triplicate until reaching equilibrium (100 minutes of reaction), and each aliquot was filtered with a 45 μ hydrophobic membrane. The concentration of degraded methyl

Table 1: Optimization by Design Expert software of aqueous extracts of *Cinnamomum verum*.

Runs	Independent variables			Response variable
	X_1 Weight of *Cinnamomum verum* (g)	X_2 Microwave irradiation power (W)	X_3 Microwave irradiation time *(s)*	Weight of *Cinnamomum verum* extract (g)
1	3.0	350	300	0.0582
2	1.5	150	600	0.0617
3	4.5	150	600	0.0902
4	3.0	350	900	0.0453
5	1.5	350	600	0.0406
6	1.5	250	300	0.0610
7	3.0	250	600	0.0535
8	3.0	250	600	0.0521
9	4.5	350	600	0.0706
10	3.0	250	600	0.0558
11	3.0	150	300	0.0511
12	1.5	250	900	0.0440
13	4.5	250	300	0.0673
14	3.0	150	900	0.0607
15	3.0	250	600	0.0542
16	4.5	250	900	0.0596
17	3.0	250	600	0.0533

orange was quantified in a Perkin Elmer brand UV-vis Lambda XLS spectrophotometer at a wavelength of 467 nm. The above procedure was repeated for the CO-TiO_2 and A-TiO_2 photocatalysts and the photolysis.

3. Results and Discussion

3.1. Cinnamomum verum Aqueous Extract Optimization. According to Table 1, the highest amount of extracts was obtained for run number 3 with 0.0902 g of bioactive, with 4.5 g of ground cinnamon, power of 150 W, and microwave irradiation time of 600 s, followed by runs 9 and 13, and the one that obtained the least amount of cinnamon extract was run 5. ANOVA results considering the second-order polynomial model of the 17 runs are shown in Tables 2 and 3.

ANOVA results predicted a quadratic model (equation (2)) for the three independent variables (weight of *Cinnamomum verum*, microwave irradiation time, and microwave irradiation power). The results in Table 2 suggested that the generated model had a high value of the coefficient of determination R squared (0.8283). The results in Table 3 indicate that the model had a high F value (3.75) and a low p value (0.0476) for the response indicating that the quadratic model is significant. This suggests that the model could predict 82% of the variations in the experimental data. In this sense, the quadratic model is significant during microwave extraction.

The analysis of variance (ANOVA) determined the following second-order polynomial model:

$$Y = 0.08 - 0.018X_1 - 1.52E10^{-4}X_2 + 0.71EX_3 + 2.5E10^{-6}X_1X_2 + 5.16E10^{-6}X_1X_3 - 1.87EX_2X_3 + 3.58E10^{-3}X_1^2 + 3.92E10^{-7}X_2^2 - 4.30EX_3^2. \quad (2)$$

Table 2: Predicted and experimental values of the responses were obtained under optimal extra extraction conditions.

Predicted model	Sum of squares	Df	R^2
Quadratic	0.0018	9	0.8283

Df: degree of freedom and R^2: coefficient of determination.

The analysis of the response surface and contour is shown in Figure 1. 3D dimensional graphs were obtained by the ANOVA for the 17 runs, and the relationship of the independent and dependent variables was studied for getting the *Cinnamomum verum* extract.

The analysis of the response surface and contour of the weight of the *Cinnamomum verum* extract shows the effect of these independent variables. It can be seen in the response surface graphs that the best results for the weight of the *Cinnamomum verum* extract tend to be red color, that is, lower microwave irradiation powers produce higher cinnamon extract weights, and the lowest value on the blue scale with higher irradiation power and lower *Cinnamomum verum* weights produces the lowest cinnamon extract weights (Figures 1(a)–1(c)).

When comparing the same weight of cinnamon and microwave irradiation power at different irradiation times at (A) 300 sec, it can be seen that the best results in terms of the greater amount of extract obtained tend to have higher cinnamon weights (4.5 g) and low microwave irradiation powers (150 W). In the case of (B) 600 sec and (C) 900 sec, the same trend can be observed. In general, the increase of the microwave irradiation time during the extraction of the bioactives promotes a decrease in the amount of extract obtained due to the degradation effect.

Preferably, when comparing the same weight of cinnamon and microwave irradiation power, the degradation of the resulting bioactives is promoted as the irradiation time increases.

Table 3: ANOVA statistics of quadratic models for the extraction yields of the weight of the *Cinnamomum verum* extract.

Source	Mean square	*F*-value	*p* value	*Significant
Model (quadratic)	0.0018	3.75	0.0476	Significant

F-value: Fisher-Snedecor distribution value, *p* value: probability value, *significant ($p < 0.05$).

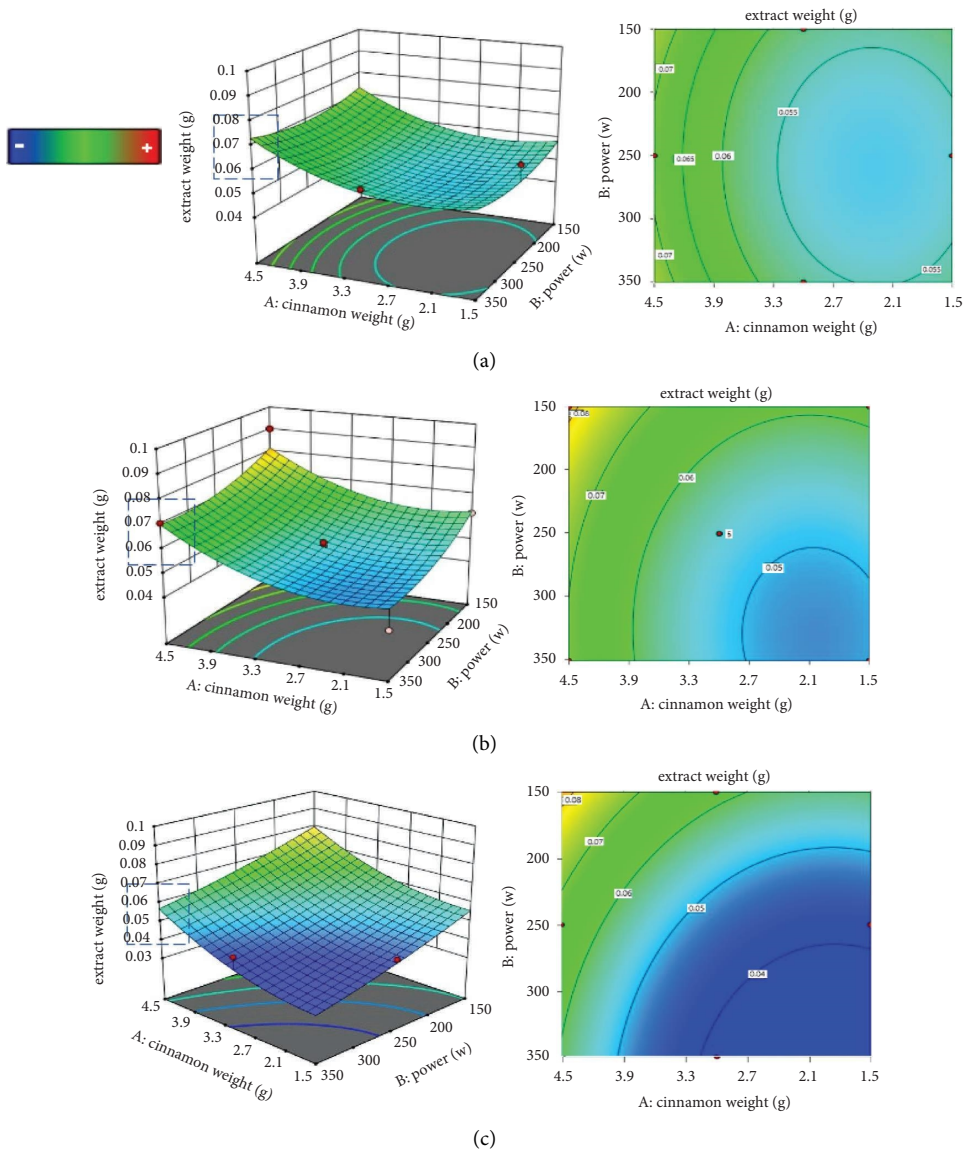

Figure 1: Analysis of response surface (ARS) and analysis of response contour, respectively: weight of *Cinnamomum verum*, microwave irradiation power vs. weight of *Cinnamomum verum* extract: (a) 300 sec, (b) 600 sec and (c) 900 sec of microwave irradiation.

Figure 2 shows the Pareto diagram, prepared with the variables X_1, X_2, and X_3 and the frequency of the response variable (amount of the *Cinnamomum verum* extract) for the 17 experiments proposed by the Design Expert program.

Based on the 80/20 Pareto principle to establish priorities in obtaining the greatest amount of the *Cinnamomum verum* extract, it corroborates the trend of the ARS graphs; that is, the greatest amount of the extract is obtained towards

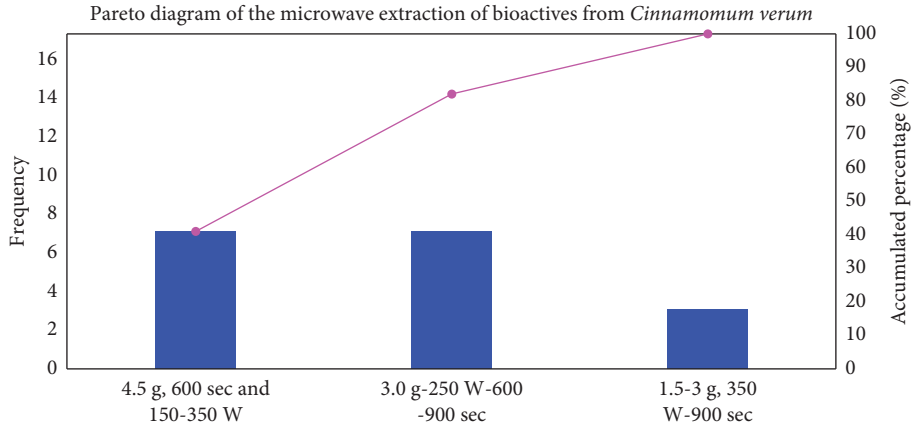

Figure 2: The Pareto diagram of the microwave extraction of bioactives from *Cinnamomum verum*.

greater weights of cinnamon (4.5 g), at low microwave irradiation powers (150 W) and an irradiation time of 600 sec [48–51].

3.2. X-Ray Diffraction (XRD). Figure 3 shows the normalized X-ray diffraction patterns of the C-TiO_2 and CO-TiO_2 samples.

Based on the JCPDS (Joint Committee on Powder Diffraction Standards) library, it can be seen that in all cases, the characteristic reflections of the anatase phase were obtained at $2\theta = 25.3$, 38.5, 48.03, 55.0, 62.11, 68.76, 75.05, and 82.16° (JCPD letter 00-021-1272) corresponding to a tetragonal unit cell. The CO-TiO_2 sample synthesized without the extract has a reflection attributed to the brookite phase (JCPD letter 01-075-2548) at $2\theta = 31°$ (B), and for the C-TiO_2 sample, two reflections are observed at $2\theta = 28$ and 42° (R) identified for the rutile crystallographic phase (JCPD letter 00-021-1276), where the commercial sample A-TiO_2 is the lowest crystallinity. Comparing the intensity of the reflections (1 0 1), (1 0 3), (2 0 0), and (1 0 5) shows that the CO-TiO_2 sample is more ordered than the C-TiO_2 sample. The crystal size was determined by the Debye–Scherrer equation. The sample synthesized by microwave and the aqueous extract of *Cinnamomum verum* (C-TiO_2) presented a smaller crystal size (1.96 nm) than the one synthesized without extract CO-TiO_2 (2.35 nm), which indicates that the phenolic and flavonoid compounds contained in the cinnamon extract promote a smaller crystal size and improve the crystallinity since both samples were synthesized under the same microwave irradiation conditions [52]. Also, the reaction time is reduced from hours to minutes (10 minutes) during the synthesis of materials with the use of microwaves.

3.3. Fourier Transform Infrared (FTIR) Spectroscopy. Figure 4 shows the absorption bands of the functional groups present in TiO_2, obtained by Fourier transform infrared (FTIR) spectroscopy for samples A-TiO_2, C-TiO_2, CO-TiO_2, and the aqueous extract of cinnamon.

In the cinnamon extract, it is possible to observe the signal corresponding to the $^{-}$OH bonds of the phenolic compounds of the extract at 3244 cm^{-1}. At 2922 cm^{-1}, the

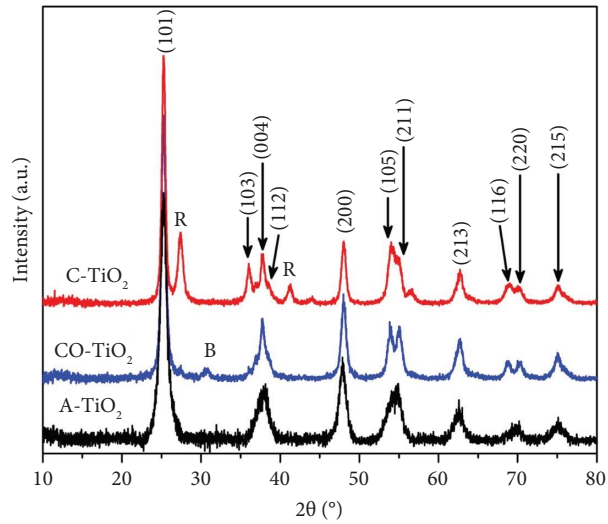

Figure 3: X-ray diffraction patterns of the C-TiO_2 and CO-TiO_2 samples. Rutile (R), and brookite (B) phases.

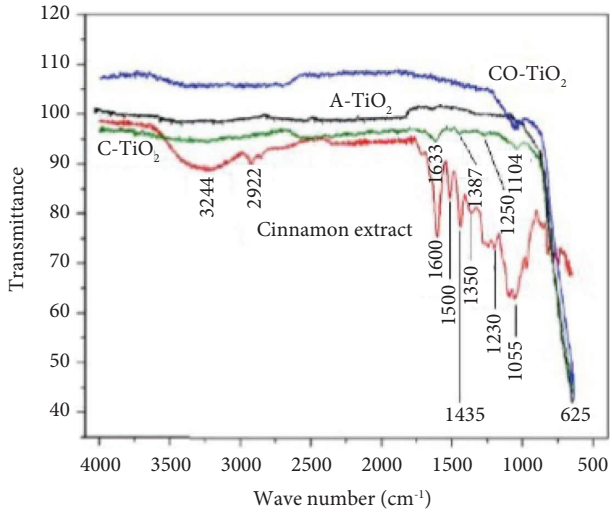

Figure 4: FTIR spectra of the samples A-TiO_2, C-TiO_2, CO-TiO_2, and the aqueous extract of cinnamon.

signal for the C-H bond of the methylene group corresponds to terpenes. The phenolic compounds appear with the absorption bands for $^{-}$COOH bonds at 1350 cm^{-1}, for C-O at 1230 and 1055 cm^{-1}, and for the flavonoids, the signals for aromatic C=O bonds are presented at 1600 cm^{-1} with its harmonics at 1500 and 1435 cm^{-1}. This indicates that the extract of *Cinnamomum verum* is composed of phenolic compounds, terpenes, and flavonoids, which have been reported to be able to promote the synthesis of TiO_2 [53].

In the case of the C-TiO_2 and CO-TiO_2 samples, the signal at 1104 cm^{-1} indicates the distribution of TiO_2 nanoparticles in the anatase phase; this has already been reported by Raghunandan et al. [54]. The additional signals that appear in the C-TiO_2 sample at 1633, 1387, and 1250 cm^{-1} could correspond to remnants of the extract.

3.4. High-Resolution Transmission Electron Microscopy. Figure 5 shows the images by bright-field micrographs (BFTEM) at different magnifications for the commercial samples A-TiO_2 (A and D) and the samples synthesized by microwave irradiation in 10 min: CO-TiO_2 (B and E) and C-TiO_2 (C and F).

At 20 and 10 nm scales, it can be seen that the sample synthesized with the *Cinnamomum verum* extract C-TiO_2 (C and F) is the one with the smallest particle size and with regular hemispherical shapes with an approximate size of 15 nm, followed by the synthesized sample without the extract CO-TiO_2 (B and E) with semielliptical irregular shapes and sizes from 20 to 40 nm and the commercial A-TiO_2 (A and D) with the least uniform shape and particle size ranging from 20 to 50 nm. At magnifications of 10 nm, it can be seen that the samples synthesized with microwaves CO-TiO_2 (E) and C-TiO_2 (F) planes of atoms with preferential orientation are observed.

Figure 6 shows the images by high-resolution transmission electron microscopy (HRTEM) at different magnifications of the C-TiO_2 sample: (A) 5 nm, (B) 1.5x, and (C) 5x. Additionally, the diffraction pattern obtained by TEM is shown in (D).

The digital enlargement of the microgram of a C-TiO_2 nanoparticle is shown (Figure 5(b)), in which the crystal lattice of this material can be observed, and the top view of the unit cell can be seen (Figure 5(c)), which corresponds to the tetragonal crystal system (marked in yellow) corresponding to the anatase phase for TiO_2, according to what was found by XRD. Therefore, the use of the aqueous extract of *Cinnamomum verum* during the synthesis assisted by microwave irradiation with titanium precursor ($TiCl_4$) promoted nanoparticles of uniform nanometric size (approximately 15 nm in diameter) with a high degree of crystallinity and preferential anatase phase. The diffraction pattern of the C-TiO_2 sample (Figure 5(d)) indicates that a polycrystalline sample of TiO_2 nanoparticles was obtained, confirming the polycrystalline nature of the material as shown in the HRTEM images (Figure (A)) [55–57].

3.5. UV-Vis Diffuse Reflectance Spectroscopy. Based on the diffuse reflectance data, it is possible to determine the optical band gap (Eg) of the A-TiO_2, C-TiO_2, and CO-TiO_2 samples using the Kubelka–Munk equation and the Tauc graphs following the formula: $\alpha h\nu = A\ (h\nu - \mathrm{Eg})^{n/2}$ for semiconductors [58–60]; these values are represented in Figure 7.

The samples synthesized by microwave irradiation with C-TiO_2 and without the CO-TiO_2 extract have a band-gap value of 3.42 and 3.67 eV, respectively, both being higher than the commercial sample A-TiO_2 brand Sigma-Aldrich (3.19 eV), which would indicate in the theory that to photoactivate the C-TiO_2 and CO-TiO_2 samples with UV light, more energy will be required, whereas the commercial sample (A-TiO_2) needs less energy to be photoactivated by UV light.

The TEM images show that the CO-TiO_2 sample has sizes between 20 and 40 nm (Figures 5(b) and 5(e)) with a band gap equal to 3.67 eV. In the case of the sample synthesized by cinnamon C-TiO_2 of 15 nm (Figures 5(c) and 5(f)), its band-gap value decreases to 3.42 eV, which indicates that there is a correspondence between the particle size and the band-gap value. This is attributed to the effect of quantum confinement of the material promoted by miniaturization, having a greater uptake of UV light absorption for the sample synthesized with the *Cinnamomum verum* extract.

3.6. Raman Spectroscopy. In Figure 8, the Raman spectra of the C-TiO_2 and CO-TiO_2 samples are presented.

In all cases, the vibrations that characterize the typical tetragonal structure of the anatase phase can be seen; the signal that appears at 450 cm^{-1} can be attributed to traces of the rutile crystallographic phase with a face-centered cubic structure, according to what is indicated in the X-ray diffraction spectra in the reflections at 28 and 42° (Figure 1) [61, 62]. The vibrations at 144 and 639 cm^{-1} are generated by the symmetric stretching of the O-Ti-O bond; the vibration at 399 cm^{-1} is caused by the symmetric bending of the O-Ti-O bonds; the vibration at 519 cm^{-1} was generated by the asymmetric bending in the O-Ti-O bond, sending signals that confirm the anatase phase as predominant in all cases [63, 64].

In Figure 9, we present a reaction proposal for the synthesis of TiO_2 using the *Cinnamomum verum* extract, based on what was proposed for the sol-gel method by Rojas et al. [65].

The synthesis of TiO_2 needs an abundance of $^{-}$OH ions; on the other hand [66], the bioactives contained in the *Cinnamomum verum* extract (mainly flavonoids and phenolic compounds) contain numerous $^{-}$OH groups in their structure [67–69], which efficiently promote a nonstable polymeric structure by hydrolysis generating $Ti(OH)_4$ and HCl, where the use of the aqueous extract of cinnamon contributes to the nucleation and growth of the polymeric phase. The resulting mixture was washed to remove HCl and

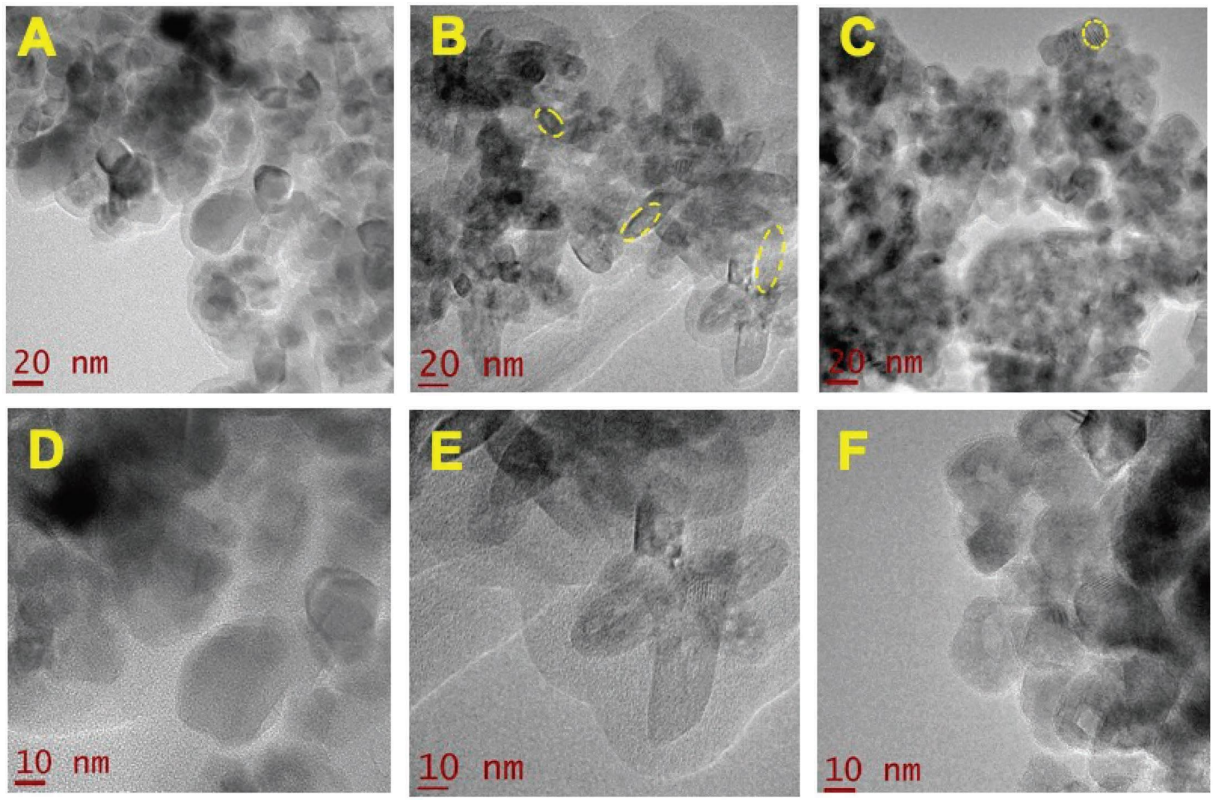

Figure 5: Bright-field transmission electron microscopy (BFTEM) micrograms for the samples: A-TiO_2 (a, d), CO-TiO_2 (b, e), and C-TiO_2 (c, f).

calcined (450°C for 4 h); after calcination, the tetragonal crystallographic structure was generated, and that corresponds to the anatase phase for the nanometric TiO_2 (Figure 7), which has a smaller particle size, more uniform size, and crystallinity than the rest of the materials evaluated (CO-TiO_2 and A-TiO_2).

3.7. Evaluation of the Adsorption-Photodegradation of Methyl Orange. Figure 10 shows the profile with the adsorption-photodegraded percentages of methyl orange at the optimal conditions for the samples C-TiO_2, CO-TiO_2, and A-TiO_2 and the photolysis (without catalyst) of the system at 3 ppm of contaminant with adsorption (15 min (a)) and degradation (100 min (b)) time of equilibrium, respectively, using a ratio of 1 g of catalyst per liter of methyl orange.

According to Figure 10(a), the sample synthesized with the *Cinnamomum verum* extract (C-TiO_2) is the one with the highest percentage of adsorption (7.5%), reaching equilibrium time experimentally in 15 min, followed by the C-TiO_2 sample (4.7%) and A-TiO_2 (1.76%). 10(b) The percentages of photodegradation for photolysis and samples A-TiO_2, CO-TiO_2, and C-TiO_2 with 100 min of UV irradiation resulted in 34.22, 81.42, 95.56, and 100%, respectively. The C-TiO_2 sample, synthesized with an aqueous extract of cinnamon (*Cinnamomum verum*), completely photodegraded methyl orange (100%) in just 40 minutes, reaching equilibrium at this time, unlike the rest of the experiments.

Figure 11 shows a comparison of the percentages of adsorption-photodegradation with all the materials evaluated with an exposure of 40 min.

The photolysis after 40 minutes only reaches up to photodegradation of 12.95%, followed by the A-TiO_2 sample (commercial) with 36.97%. For the samples synthesized with $TiCl_4$, with the aqueous extract of *Cinnamomun verum* and microwave irradiation (C-TiO_2), there is an improvement of 52.22% of methyl orange photodegradation when compared with CO-TiO_2. This can be attributed primarily to the fact that the band gap for the C-TiO_2 sample (Eg = 3.42 eV) is lower than that for the CO-TiO_2 sample (Eg = 3.67 eV), indicating that less energy is required to pass electrons from the valence band to the conduction band. In addition, the particle size was smaller, and the crystallinity was higher than the synthesized sample without extract; therefore, the active sites of the catalyst were better exposed than the sample synthesized without the extract. Other authors have found that there could be traces of the bioactives used as precursors (corroborated by FTIR, Figure 3), which could additionally have a photochromic effect and facilitate the photoreaction [66]. Additionally, when quantifying the adsorption of the dye, it can be seen that the resulting

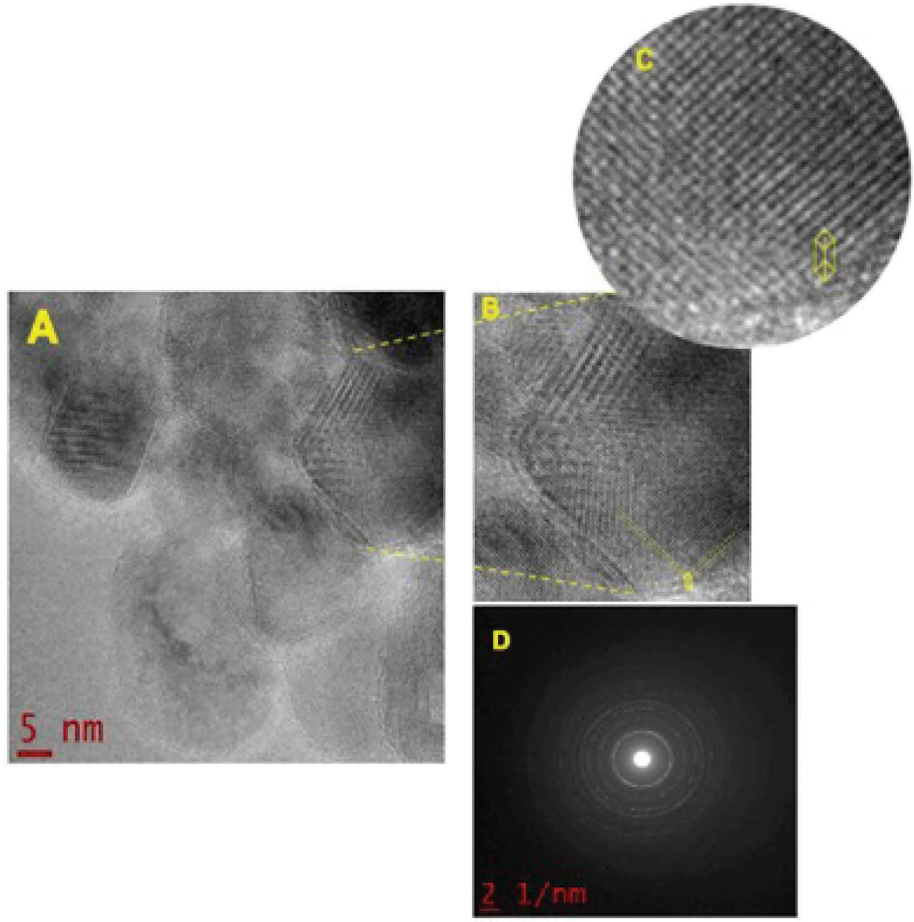

Figure 6: Micrograms by high-resolution transmission electron microscopy (HRTEM) for the C-TiO_2 sample at (a) 5 nm, (b) 1.5x, and (c) 5x. (d) Diffraction pattern obtained by TEM.

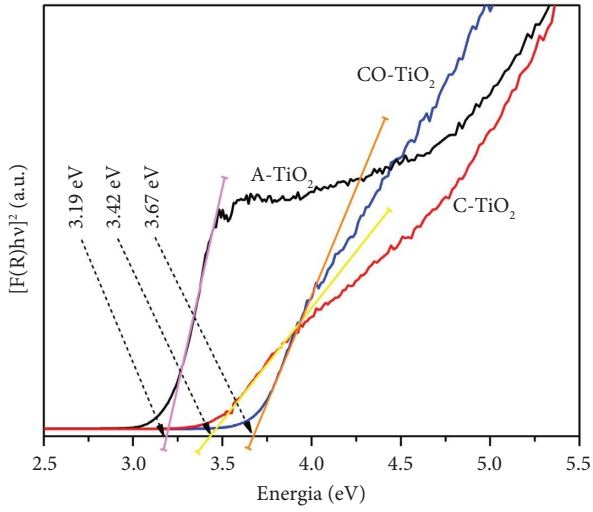

Figure 7: Diffuse reflectance spectra for A-TiO_2 photocatalysts, C-TiO_2, and CO-TiO_2.

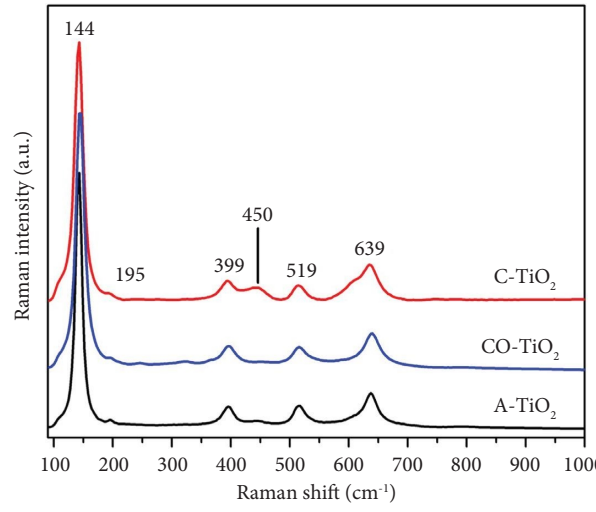

Figure 8: Raman spectra of the C-TiO_2 and CO-TiO_2 samples.

morphology for the C-TiO_2 sample allowed a better interaction of the catalyst with the reaction medium, contributing to the photodegradation (Figure 5(f)).

In the comparison of the C-TiO_2 (15 nm) and A-TiO_2 (50 nm) samples, the smaller particle size of the sample prepared with extract allowed for the exposure of a greater number of active sites in photodegradation, in addition to

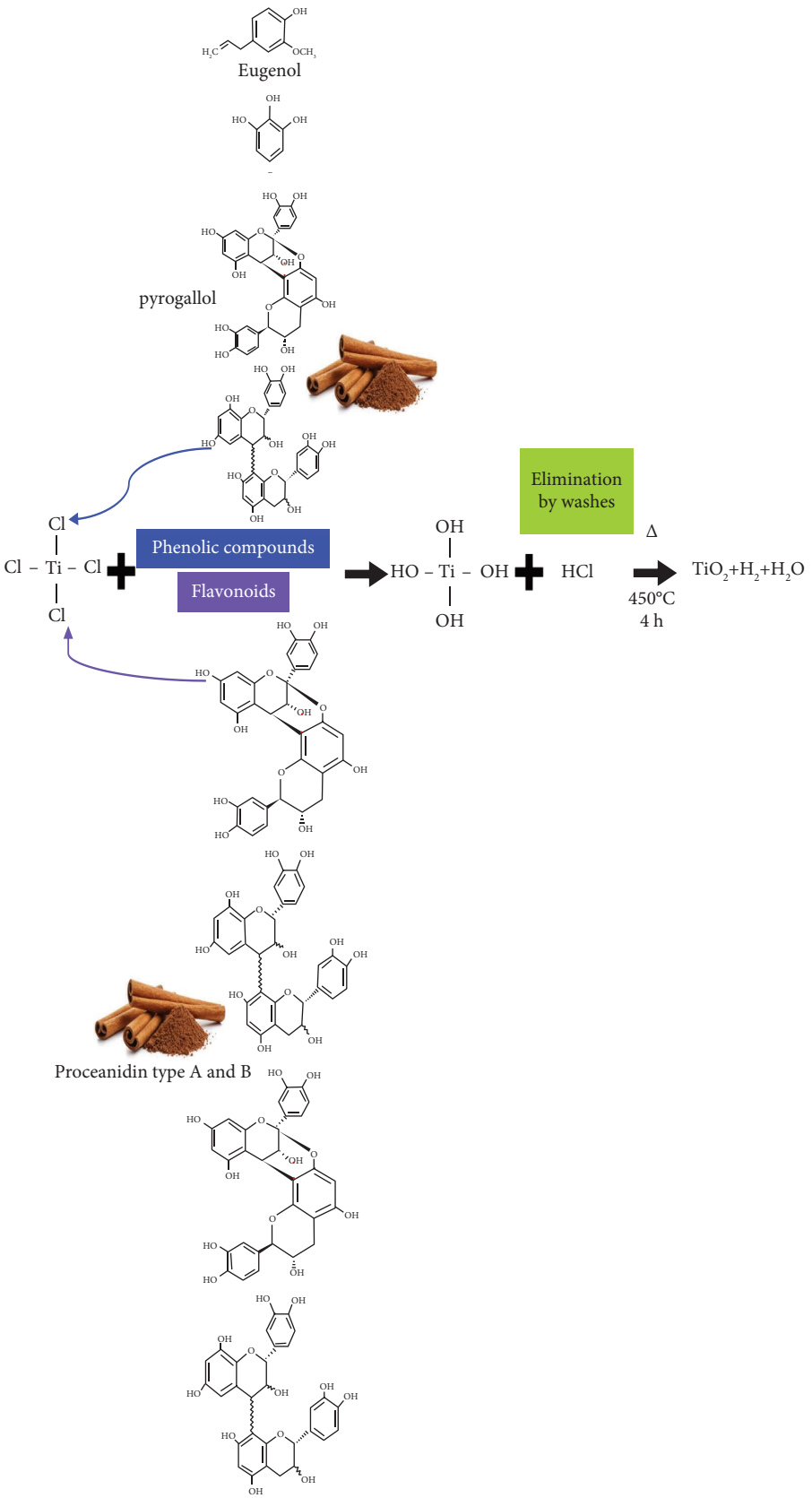

Figure 9: Reaction proposal to obtain nanometric TiO_2 using the *Cinnamomum verum* extract.

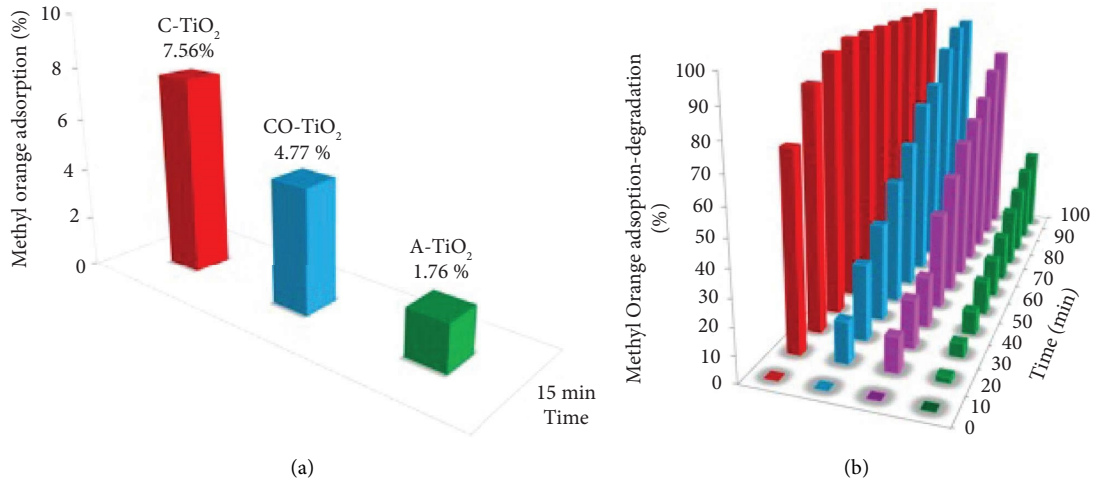

Figure 10: Methyl orange adsorption-photodegradation profiles, with 15 minutes (a) of adsorption and 100 minutes (b) of photodegradation for the samples CO-TiO_2, C-TiO_2, A-TiO_2, and the photolysis of the system.

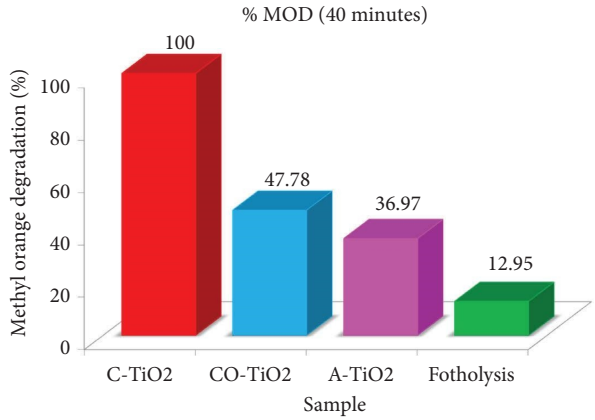

Figure 11: Percentage of adsorption-photodegradation of methyl orange (% MOD) at 40 minutes of reaction for the samples CO-TiO_2, C-TiO_2, A-TiO_2, and the photolysis of the system.

the already mentioned photochromic effect. Therefore, the sample synthesized with the aqueous cinnamon extract, despite having a higher band gap (Eg = 3.42 eV), was more photoactive than the commercial sample (Eg = 3.19 eV).

Figure 12, (A) shows the values obtained for the constant rate (k (min^{-1})) and the order (n) of the reaction calculated for the adsorption-degradation of methyl orange. Sections (B) to (C) present the speed profiles ($-r_{\text{methyl orange adsorption-degradation}}$) for the evaluated samples.

In all cases, the adjustment of the speed model (ppm methyl orange/min) corresponds to order one ($n = 1$), where the speed constants (k) resulted in values of $k = 0.89$, 0.021, 0.012, and 0.003 min^{-1} for the samples C-TiO_2, CO-TiO_2, A-TiO_2, and the photolysis of the system, respectively, with R^2 settings between 0.89 and 0.99 (Figure 12(a)). These values can be corroborated in the speed profiles (Figures 12(b) and 12(c)), where the sample synthesized with the *Cinnamomum verum* extract is the one with the highest speed according to the highest value of k of the tested materials, which shows the excellent interaction of TiO_2 with the reaction medium, attributable to the higher adsorption of methyl orange in the C-TiO_2 sample; therefore, the C-TiO_2 sample has smaller crystal size, smaller particle size, higher crystallinity, and smaller band gap than the one synthesized without cinnamon.

Figure 13 shows the UV-vis spectra obtained for the remnants of the sorption photodegradation of methyl orange to identify intermediate products, using the semiconductor CO-TiO_2 (%MOD = 95.56), that did not reach total mineralization after 40 and 100 min of photodegradation.

In the spectrum at the beginning of the reaction (0 min), two signals are presented. The first is located at $\lambda = 466$ nm, which is indicative of the chromophore group -N=N- (azo); the second signal at $\lambda = 269$ nm is associated with the benzene rings in the methyl orange structure. After 40 min of irradiation with UV light, the signal at 466 nm reduces its intensity, and after 100 min of irradiation, it disappears; this indicates the breaking of the -N=N group bond [70, 71]. In the case of the signal at 269 nm, it can be observed that after 40 min of irradiation it decreased, and at 100 min, a displacement of the signal is observed at approximately 253 nm, which indicates that the aromatic group was not fractionated, generating by-products derived from the aromatic ring which can be attributed to N,N-dimethyl-p-phenylenediamine, as reported by Lide and Col. [72] and sulfanilic acid in [73]. It is worth mentioning that the C-TiO_2 sample does not show any signal after photodegradation, and it is likely that it has reached mineralization.

Table 4 shows a comparison of studies where TiO_2 was used for the degradation of methyl orange compared to TiO_2 synthesized with the *Cinnamomum verum* extract.

Fortunately, the C-TiO_2 sample being a pristine material shows a very good percentage of degradation in a short time compared to binary and ternary materials (Table 4). So, the green synthesis of nanostructures such as C-TiO_2 represents an area of opportunity for the synthesis of more efficient materials since it can be coupled with other semiconductors and graphitic materials and decorated or doped with metals.

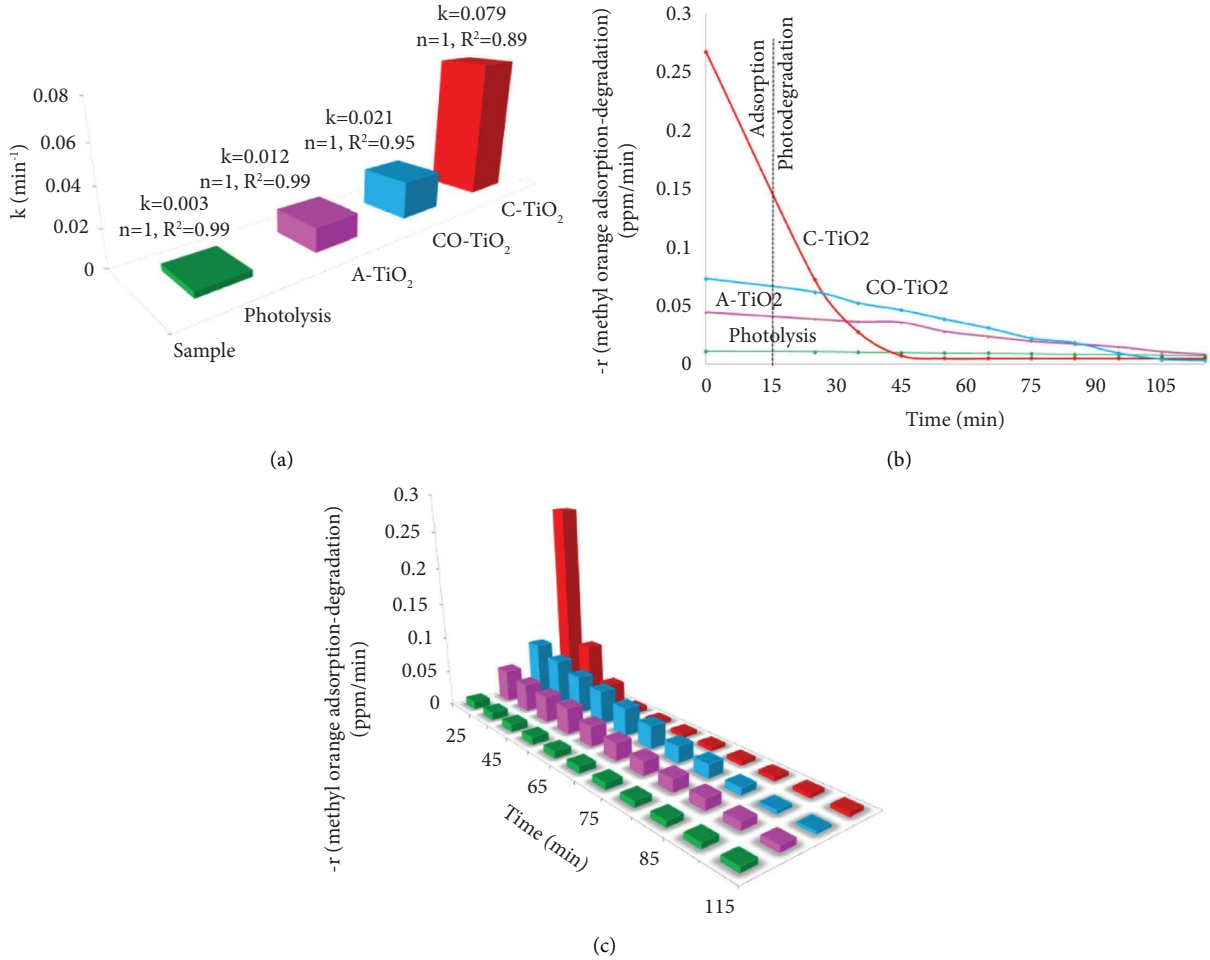

FIGURE 12: (a) Values obtained for the constant rate (k/min^{-1}) and order of the reaction ($n = 1$). (b, c) Rate profiles ($-r_{\text{methyl orange adsorption-degradation}}$) for the samples CO-$TiO_2$, C-$TiO_2$, A-$TiO_2$, and the photolysis of the system.

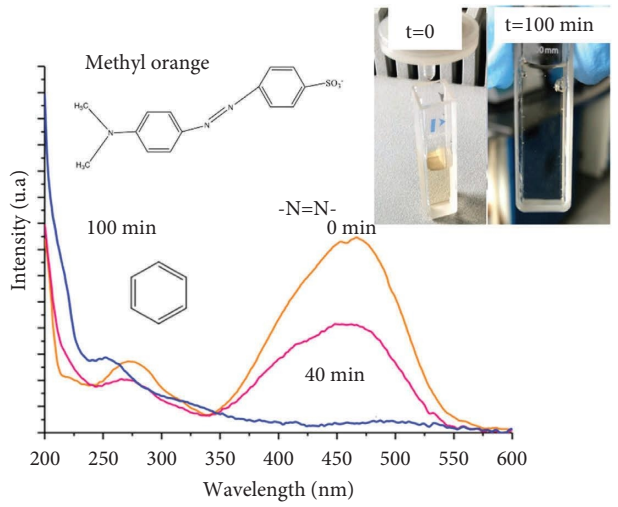

FIGURE 13: UV-vis spectra were obtained for the remnants of the sorption photodegradation of methyl orange, using CO-TiO_2 after 40 and 100 minutes of photodegradation.

Table 4: Comparison of different studies with the presence of TiO_2 synthesized with the *Cinnamomum verum* extract.

Photocatalyst	Synthesis method	Conditions	Removal efficiency (%)	Reference
$CuFeS_2$@ TiO_2	Mechanochemical route	Methyl orange visible light	Ca. 74% @ $t = 120$ min	[74]
Palygorskite/UiO-66- TiO_2	Wet chemical process	Methyl orange UV irradiation	100% @ $t < 120$ min	[75]
$ZnFe_2O_4$@TiO_2	Solvothermal-US assisted	Methyl orange UV irradiation	83.8% @ $t = 60$ min	[76]
Submicrometer TiO_2	Sol-gel/annealing	Methyl orange UV irradiation	Ca. 70% @ $t = 160$ min	[77]
TiO_2@CS-PANI	Process of polymerization	Methyl orange visible light	89.5% @ $t = 50$ min	[78]
Ag/TiO_2/carbon	Hydrothermal	Methyl orange visible light	94% @ $t = 100$ min	[79]
SnO_2/TiO_2	Hydrothermal	Methyl orange xenon lamp	91% @ $t = 120$ min	[80]
PTF- TiO_2	Composite solution with water spray	Methyl orange UVA irradiation	100% @ $t = 120$ min	[81]
C-TiO_2CO-TiO_2	Microwave irradiation	Methyl orange UV irradiation	100% @ $t = 40$ min 40% @ $t = 40$ min	This work

4. Conclusions

The optimization of the aqueous extract of *Cinnamomum verum* predicts a significant quadratic model, with an 82% prediction to the experimental variations.

It was feasible to synthesize nanocrystalline solids of the TiO_2 anatase phase by microwave irradiation for 10 minutes at 150 watts of power, with and without the aqueous extract of *Cinnamomum verum*, where the size of the particle is influenced by the bioactive during the synthesis (the aqueous extract of *Cinnamomum verum*) and the synthesis method (microwave irradiation), resulting in smaller size and crystallinity when synthesized with the aqueous extract of cinnamon.

The signals obtained in the FTIR spectrogram for the aqueous extract of *Cinnamomum verum* suggest the presence of terpenes, phenolic compounds, and flavonoids. For the samples A-TiO_2, C-TiO_2, and CO-TiO_2, the vibration modes of the Ti-O and Ti-O-Ti bonds are confirmed with the signal at 625 cm^{-1}. For the C-TiO_2 and CO-TiO_2 samples, the signal at 1104 cm^{-1} confirms the formation of TiO_2 nanoparticles in the anatase phase since this signal does not appear in the A-TiO_2 sample.

The use of the aqueous extract of *Cinnamomum verum* FIGURAS FIONALES promotes during the synthesis of TiO_2 that the value of the band gap decreases, affects the crystallinity, and decreases the size of the crystal, compared to the sample synthesized without the extract (CO-TiO_2) since both were prepared under the same synthesis conditions.

Raman spectroscopy confirms that the C-TiO_2 and CO-TiO_2 samples mostly contain the tetragonal crystallographic structure corresponding to the anatase phase. In both cases, the presence of traces of the face-centered cubic crystallographic structure of the rutile phase is also confirmed.

The commercial sample A-TiO_2 does not have a good particle size uniformity, where larger size particles predominate (50 nm). The sample synthesized by microwave irradiation without the extract promoted the formation of elliptical nanoparticles with good uniformity and sizes of approximately 20 nm in diameter. When using an aqueous extract of *Cinnamomum verum* during the synthesis, it generated a material with a uniform particle size (less than 15 nm in diameter), with a higher degree of crystallinity.

The use of the aqueous extract of cinnamon (*Cinnamomum verum*) during the synthesis of TiO_2 generated a semiconductor with a smaller crystal size, smaller particle size, higher crystallinity, smaller band gap, and greater adsorption capacity for the dye tested as a reaction model (methyl orange) than the one synthesized without cinnamon, which apparently promotes the total mineralization of methyl orange in 40 minutes of reaction, making it the best material of those evaluated in the adsorption-photodegradation.

Data Availability

The experimental data used to support the findings of this study are available from the corresponding author upon request.

Conflicts of Interest

The authors declare that they have no conflicts of interest.

Acknowledgments

The authors wish to thank the "Instituto Politécnico Nacional" for funding this research through the SIP 2022 1522, SIP 2022 0908, and SIP2022 1671 projects.

References

[1] S. K. Srikar, D. D. Giri, D. B. Pal, P. K. Mishra, and S. N. Upadhyay, "Green synthesis of silver nanoparticles: a review," *Green and Sustainable Chemistry*, vol. 06, no. 1, pp. 34–56, 2016.

[2] N. Jayarambabu, A. Akshaykranth, T. Venkatappa Rao, K. Venkateswara Rao, and R. Rakesh Kumar, "Green synthesis of Cu nanoparticles using Curcuma longa extract and their application in antimicrobial activity," *Materials Letters*, vol. 259, no. 15, Article ID 126813, 2020.

[3] J. M. Abisharani, S. Devikala, R. D. Kumar, M. Arthanareeswari, and P. Kamaraj, "Green synthesis of TiO2 nanoparticles using Cucurbita pepo seeds extract," *Materials Today: Proceedings*, vol. 14, no. 2, pp. 302–307, 2019.

[4] E. Tilahun Bekele, B. A. Gonfa, and F. K. Sabir, "Use of different natural products to control growth of titanium oxide nanoparticles in green solvent emulsion characterization, and their photocatalytic application," *Bioinorganic Chemistry and Applications*, vol. 2021, Article ID 6626313, 17 pages, 2021.

[5] S. Syamsol Bahri, Z. Harun, S. Khadijah Hubadillah et al., "Review on recent advance biosynthesis of TiO2 nanoparticles from plant-mediated materials: characterization, mechanism and application," *IOP Conference Series: Materials Science and Engineering*, vol. 1142, no. 1, p. 12005, 2021.

[6] P. Sathishkumar, F. L. Gu, Q. Zhan, T. Palvannan, and A. R. Mohd Yusoff, "Flavonoids mediated 'Green' nanomaterials: a novel nanomedicine system to treat various diseases current trends and future perspective," *Materials Letters*, vol. 210, no. 1, pp. 26–30, 2018.

[7] W. W. Andualem, F. K. Sabir, E. T. Mohammed, H. H. Belay, and B. A. Gonfa, "Synthesis of copper oxide nanoparticles using plant leaf extract of Catha edulis and its antibacterial activity," *Journal of Nanotechnology*, vol. 2020, Article ID 2932434, 10 pages, 2020.

[8] K. E. Rivas Mena, D. L. Muñoz, C. N. Pino Benítez, and N. Balcázar Morales, "Actividad antioxidante, contenido fenólico total y citotoxicidad de extractos polares obtenidos de plantas antidiabéticas colombianas Antioxidant activity, total phenolic content and cytotoxicity of polar extracts from Colombian antidiabetic plants," *Revista Cubana de Plantas Medicinales*, vol. 20, no. 3, pp. 277–289, 2015.

[9] A. Rana, K. Yadav, and S. Jagadevan, "A comprehensive review on green synthesis of nature-inspired metal nanoparticles: mechanism, application and toxicity," *Journal of Cleaner Production*, vol. 272, no. 1, Article ID 122880, 2020.

[10] H. Veisi, R. Ghorbani-Vaghei, S. Hemmati, M. H. Aliani, and T. Ozturk, "Green and effective route for the synthesis of monodispersed palladium nanoparticles using herbal tea extract (Stachys lavandulifolia) as reductant, stabilizer and capping agent, and their application as homogeneous and reusable catalyst in Suzuki coupling reactions water," *Applied Organometallic Chemistry*, vol. 29, no. 1, pp. 26–32, 2015.

[11] Y. Orooji, S. Mortazavi-Derazkola, S. M. Ghoreishi, M. Amiri, and M. Salavati-Niasari, "Mesopourous Fe3O4@SiO2 hydroxyapatite nanocomposite: green sonochemical synthesis using strawberry fruit extract as a capping agent, characterization and their application in sulfasalazine delivery and cytotoxicity," *Journal of Hazardous Materials*, vol. 400, no. 5, Article ID 123140, 2020.

[12] N. Singh, A. S. Rao, A. Nandal et al., "Phytochemical and pharmacological review of Cinnamomum verum J Presl-a versatile spice used in food and nutrition," *Food Chemistry*, vol. 338, no. 15, Article ID 127773, 2021.

[13] R. Pathak and H. Sharma, "A review on medicinal uses of Cinnamomum verum (cinnamon)," *Journal of Drug Delivery and Therapeutics*, vol. 11, no. 6, pp. 161–166, 2021.

[14] R. Souto da Rosa, R. Numata, and M. E. Marovic, "Análisis micrográfico y fitoquímico de muestras comerciales de "canela" - micrographic and phytochemical analysis of commercial samples of "Cinnamomum verum"," *Dominguezia*, vol. 31, no. 2, pp. 11–15, 2015.

[15] S. P. Goutam, G. Saxena, V. Singh, A. K. Yadav, R. N. Bharagava, and K. B. Thapa, "Green synthesis of TiO2 nanoparticles using leaf extract of Jatropha curcas L for photocatalytic degradation of tannery wastewater," *Chemical Engineering Journal*, vol. 336, no. 15, pp. 386–396, 2018.

[16] Y. C. Liu, Y. F. Lu, Y. Z. Zeng, C. H. Liao, J. C. Chung, and T. Y. Wei, "Nanostructured mesoporous titanium dioxide thin film prepared by sol-gel method for dye-sensitized solar cell," *International Journal of Photoenergy*, vol. 2011, Article ID 619069, 9 pages, 2011.

[17] I. Iavicoli, V. Leso, and A. Bergamaschi, "Toxicological effects of titanium dioxide nanoparticles a review of in vivo studies," *Journal of Nanomaterials*, vol. 2012, Article ID 964381, 36 pages, 2012.

[18] E. Mosquera, N. Rosas, A. Debut, and V. H. Guerrero, "Síntesis y caracterización de Nanopartículas de dióxido de titanio obtenidas por el método de Sol-Gel," *Revista Politécnica*, vol. 36, no. 3, pp. 1–7, 2015.

[19] C. P. Betancur Henao, V. Hernández Montes, and R. Buitrago Sierra, "Nanopartículas para materiales antibacterianos y aplicaciones del dióxido de titanio," *Revista Cubana de Investigaciones Biomédicas*, vol. 35, no. 4, pp. 387–402, 2016.

[20] B. Saha, S. Kumar, and S. Sengupta, "Green synthesis of nano silver on TiO2 catalyst for application in oxidation of thiophene," *Chemical Engineering Science*, vol. 199, no. 18, pp. 332–341, 2019.

[21] M. Atarod, M. Nasrollahzadeh, and S. Mohammad Sajadi, "Euphorbia heterophylla leaf extract mediated green synthesis of Ag/TiO2 nanocomposite and investigation of its excellent catalytic activity for reduction of variety of dyes in water," *Journal of Colloid and Interface Science*, vol. 462, no. 15, pp. 272–279, 2016.

[22] P. Barone, F. Stranges, M. Barberio, D. Renzelli, A. Bonanno, and F. Xu, "Study of band gap of silver nanoparticles - titanium dioxide nanocomposites," *Journal of Chemistry*, vol. 2014, Article ID 589707, 6 pages, 2014.

[23] J. Fei and J. Li, "Controlled preparation of porous TiO2-Ag nanostructures through supramolecular assembly for plasmon-enhanced photocatalysis," *Advanced Materials*, vol. 27, no. 2, pp. 314–319, 2015.

[24] I. N. Isnaeni, D. Indriyati, D. Sumiarsa, D. Sumiarsa, and I. Primadona, "Green synthesis of different TiO2 nanoparticle phases using mango-peel extract," *Materials Letters*, vol. 294, no. 1, Article ID 129792, 2021.

[25] G. V. Khade, M. B. Suwarnkar, N. L. Gavade, and K. M. Garadkar, "Green synthesis of TiO2 and its photocatalytic activity," *Journal of Materials Science: Materials in Electronics*, vol. 26, no. 5, pp. 3309–3315, 2015.

[26] I. S. Rodríguez-Clavel, S. P. Paredes-Carrera, S. O. Flores-Valle, E. J. Paz-García, J. C. Sánchez-Ochoa, and R. M. Pérez-Gutiérrez, "Effect of microwave or ultrasound irradiation in the extraction from feather keratin," *Journal of Chemistry*, vol. 2019, Article ID 1326063, 9 pages, 2019.

[27] E. J. Paz-García, S. P. Paredes-Carrera, S. O. Flores-Valle, I. S. Rodríguez-Clavel, J. C. Sánchez-Ochoa, and R. M. Pérez-Gutiérrez, "Synthesis of CuO for microwave-assisted pyrolysis of biomass," *Applied Sciences*, vol. 9, no. 24, pp. 5525–5613, 2019.

[28] M. Nüchter, B. Ondruschka, W. Bonrath, and A. Gum, "Microwave assisted synthesis – a critical technology overview," *Green Chemistry*, vol. 6, no. 3, pp. 128–141, 2004.

[29] K. Karthik, S. Dhanuskodi, S. Prabu Kumar, C. Gobinath, and S. Sivaramakrishnan, "Microwave assisted green synthesis of MgO nanorods and their antibacterial and anti-breast cancer activities," *Materials Letters*, vol. 206, no. 1, pp. 217–220, 2017.

[30] M. Tsuji, "Microwave-assisted synthesis of metallic nanomaterials in liquid phase," *ChemistrySelect*, vol. 2, no. 2, pp. 805–819, 2017.

[31] I. Bilecka and M. Niederberger, "Microwave chemistry for inorganic nanomaterials synthesis," *Nanoscale*, vol. 2, no. 8, pp. 1358–1374, 2010.

[32] T. A. Saleh and V. K. Gupta, "Photo-catalyzed degradation of hazardous dye methyl orange by use of a composite catalyst consisting of multi-walled carbon nanotubes and titanium dioxide," *Journal of Colloid and Interface Science*, vol. 371, no. 1, pp. 101–106, 2012.

[33] S. Al-Qaradawi and S. R. Salman, "Photocatalytic degradation of methyl orange as a model compound," *Journal of Photochemistry and Photobiology A Chemistry*, vol. 148, no. 1-3, pp. 161–168, 2002.

[34] E. A. Almaamary, S. R. S. Abdullah, H. A. Hasan, N. I. Ismail, R. A. A. Rahim, and M. Idris, "Plant-assisted remediation of wastewater contaminated with methyl orange using Scirpus grossus," *Journal of Environmental Biology*, vol. 40, no. 3, pp. 515–523, 2019.

[35] K. K. Karukstis, D. A. Savin, C. T. Loftus, and N. D. Angelo, "Spectroscopic studies of the interaction of methyl orange with cationic alkyltrimethylammonium bromide surfactants," *Journal of Colloid and Interface Science*, vol. 203, no. 1, pp. 157–163, 1998.

[36] P. Dinh Du, H. Thanh Danh, P. Ngoc Hoai, N. M. Thanh, V. Thang Nguyen, and D. Quang Khieu, "Heterogeneous UV/Fenton-Like degradation of methyl orange using iron terephthalate MIL-53 catalyst," *Journal of Chemistry*, vol. 2020, Article ID 1474357, 13 pages, 2020.

[37] S. Slassi, A. Fix-Tailler, G. Larcher, A. Amine, and A. El-Ghayoury, "Imidazole and azo-based schiff bases ligands as highly active antifungal and antioxidant components," *Heteroatom Chemistry*, vol. 2019, Article ID 6862170, 8 pages, 2019.

[38] J. R. Wagner, E. M. Mount, and H. F. Giles, "Design of experiments," in *Extrusion*Elsevier, Amsterdam, Netherlands, 2014.

[39] P. Sahoo and T. K. Barman, "ANN modelling of fractal dimension in machining," *Mechatronics and Manufacturing Engineering*, pp. 159–226, 2012.

[40] I. Savic, D. Gajic, S. Stojiljkovic, I. Savic, and S. di Gennaro, *Modelling and optimization of methylene blue adsorption from*

aqueous solution using bentonite clay, Vol. 33, Elsevier, Amsterdam, Netherlands, 2014.

[41] H. S. Kusuma and M. Mahfud, "Box Behnken design for investigation of microwave-assisted extraction of patchouli oil," *AIP Conference Proceedings*, vol. 1699, Article ID 050014, 2015.

[42] H. S. Kusuma, R. G. M. Sudrajat, D. F. Susanto, S. Gala, and M. Mahfud, "Response surface methodology (RSM) modeling of microwave-assisted extraction of natural dye from Swietenia mahagony: a comparation between Box-Behnken and central composite design method," *AIP Conference Proceedings*, vol. 1699, p. 50009, 2015.

[43] H. S. Kusuma, M. E. Syahputra, D. Parasandi, A. Altway, and M. Mahfud, "Optimization of microwave hydrodistillation of dried patchouli leaves by response surface methodology," *Rasayan Journal of Chemistry*, vol. 10, no. 3, pp. 861–865, 2017.

[44] A. Ansori, S. A. Wibowo, H. S. Kusuma, D. S. Bhuana, and M. Mahfud, "Production of biodiesel from nyamplung (Calophyllum inophyllum L.) using microwave with CaO catalyst from eggshell waste: optimization of transesterification process parameters," *Open Chemistry*, vol. 17, no. 1, pp. 1185–1197, 2019.

[45] H. S. Kusuma, A. N. Amenaghawon, H. Darmokoesoemo et al., "Evaluation of extract of Ipomoea batatas leaves as a green coagulant–flocculant for turbid water treatment: parametric modelling and optimization using response surface methodology and artificial neural networks," *Environmental Technology and Innovation*, vol. 24, Article ID 102005, 2021.

[46] H. S. Kusuma, A. N. Amenaghawon, H. Darmokoesoemo et al., "A comparative evaluation of statistical empirical and neural intelligence modeling of Manihot esculenta-derived leaves extract for optimized bio-coagulation-flocculation of turbid water," *Industrial Crops and Products*, vol. 186, Article ID 115194, 2022.

[47] O. D. Fagbemi, B. Sithole, and T. Tesfaye, "Optimization of keratin protein extraction from waste chicken feathers using hybrid pre-treatment techniques," *Sustainable Chemistry and Pharmacy*, vol. 17, Article ID 100267, 2020.

[48] A. P. Sarmento, A. C. Borges, A. T. D. Matos, and L. L. Romualdo, "Sulfamethoxazole and trimethoprim degradation by Fenton and Fenton-like processes," *Water (Switzerland)*, vol. 12, no. 6, p. 1655, 2020.

[49] S. Choudhary, K. Sharma, M. S. Bhatti, V. Sharma, and V. Kumar, "DOE-based synthesis of gellan gum-acrylic acid-based biodegradable hydrogels: screening of significant process variables and in situ field studies," *RSC Advances*, vol. 12, no. 8, pp. 4780–4794, 2022.

[50] E. O. Marson, V. A. B. de Paiva, B. R. Gonçalves et al., "Degradation of Direct Red 81 mediated by Fenton reactions: multivariate optimization, effect of chloride and sulfate, and acute ecotoxicity assessment," *Environmental Science and Pollution Research*, vol. 24, no. 7, pp. 6176–6186, 2017.

[51] M. Bagal, G. Kumbhar, S. Shukla, A. Tiwari, D. Gajbhiye, and A. Mohod, "Degradation of dye in a continuous zig-zag flow pattern photocatalytic reactor using a Doehlert matrix," *Chemical Engineering Research and Design*, vol. 188, pp. 315–329, 2022.

[52] J. Flores-Cantera, J. A. Cruz-Mérida, F. D. Velázquez-Herrera, S. P. Paredes-Carrera, and Y. Zarazua-Aguilar, "Synchronous microwave and ultrasound irradiation for the synthesis of SBA-15," *MRS Communications*, vol. 12, no. 3, pp. 388–393, 2022.

[53] M. N. Lakhan, R. Chen, A. H. Shar et al., "Eco-friendly green synthesis of clove buds extract functionalized silver nanoparticles and evaluation of antibacterial and antidiatom activity," *Journal of Microbiological Methods*, vol. 173, Article ID 105934, 2020.

[54] D. Raghunandan, P. A. Borgaonkar, B. Bendegumble et al., "Microwave-assisted rapid extracellular biosynthesis of silver nanoparticles using carom seed (Trachyspermum copticum) extract and in vitro studies," *American Journal of Analytical Chemistry*, vol. 02, no. 04, pp. 475–483, 2011.

[55] P. C. Nethravathi, Udayabhanu, G. Nagaraju, and D. Suresh, "TiO2 and Ag-TiO2 nanomaterials for enhanced photocatalytic and antioxidant activity: green synthesis using Cucumis melo juice," *Materials Today: Proceedings*, vol. 49, pp. 841–848, 2022.

[56] M. Michalska, J. Pavlovský, K. Lemański et al., "The effect of surface modification with Ag nanoparticles on 21 nm TiO2: anatase/rutile material for application in photocatalysis," *Materials Today Chemistry*, vol. 26, Article ID 101123, 2022.

[57] R. J. Kamble, P. V. Gaikwad, K. M. Garadkar, S. R. Sabale, V. R. Puri, and S. S. Mahajan, "Photocatalytic degradation of malachite green using hydrothermally synthesized cobalt-doped TiO2 nanoparticles," *Journal of the Iranian Chemical Society*, vol. 19, no. 1, pp. 303–312, 2022.

[58] N. Qutub, P. Singh, S. Sabir, S. Sagadevan, and W. C. Oh, "Enhanced photocatalytic degradation of Acid Blue dye using CdS/TiO2 nanocomposite," *Scientific Reports*, vol. 12, no. 1, pp. 5759–5818, 2022.

[59] A. K. Manna, S. R. Joshi, B. Satpati et al., "Influence of ion implantation on depth dependent phase transition in TiO2 films, anatase nanostructures and photo-absorption behavior," *Current Applied Physics*, vol. 43, pp. 1–8, 2022.

[60] T. Zhu and S.-P. Gao, "The stability, electronic structure, and optical property of TiO2 polymorphs," *Journal of Physical Chemistry C*, vol. 118, no. 21, pp. 11385–11396, 2014.

[61] X. Zhang, J. Zhao, A. V. Whitney, J. W. Elam, and R. P. van Duyne, "Ultrastable substrates for surface-enhanced Raman spectroscopy: Al 2O3 overlayers fabricated by atomic layer deposition yield improved anthrax biomarker detection," *Journal of the American Chemical Society*, vol. 128, no. 31, pp. 10304–10309, 2006.

[62] A. di Paola, M. Bellardita, and L. Palmisano, "Brookite, the least known TiO2 photocatalyst," *Catalysts*, vol. 3, no. 1, pp. 36–73, 2013.

[63] J. F. Li, X. D. Tian, S. B. Li et al., "Surface analysis using shell-isolated nanoparticle-enhanced Raman spectroscopy," *Nature Protocols*, vol. 8, no. 1, pp. 52–65, 2013.

[64] K. Vajda, K. Saszet, E. Z. Kedves et al., "Shape-controlled agglomeration of TiO2 nanoparticles. New insights on polycrystallinity vs. single crystals in photocatalysis," *Ceramics International*, vol. 42, no. 2, pp. 3077–3087, 2016.

[65] V. C. M. Rojas, L. Matejova, A. López Milla, and G. J. Cruz, "Obtención de partículas de TiO2 por sol-gel, asistido con ultrasonido para aplicaciones fotocatalíticas," *Revista de la Sociedad Quimica del Peru*, vol. 81, no. 3, pp. 201–211, 2015.

[66] E. I. Moreno Valencia, S. P. Paredes Carrera, J. C. Sánchez Ochoa, S. O. Flores Valle, and J. R. Avendaño Gómez, "Diclofenac degradation by heterogeneous photocatalysis with Fe_3O_4/Ti $_x$ O $_y$ /activated carbon fiber composite synthesized by ultrasound irradiation," *Materials Research Express*, vol. 4, no. 11, Article ID 115026, 2017.

[67] L. B. de Lima, W. A. Viturino da Silva, S. L. Silva et al., "Chemical and antibacterial analysis of Cinnamomum verum leaves extract and fractions against multidrug resistant

bacteria," *Natural Product Research*, vol. 36, no. 10, pp. 2559–2564, 2022.

[68] R. M. Pérez Gutiérrez, F. F. Martínez Jerónimo, J. G. Contreras Soto, A. Muñiz Ramírez, and M. F. Estrella Mendoza, "Optimization of ultrasonic-assisted extraction of polyphenols from the polyherbal formulation of Cinnamomum verum, Origanum majorana, and Origanum vulgare and their anti-diabetic capacity in zebrafish (Danio rerio)," *Heliyon*, vol. 8, no. 1, p. 08682, 2022.

[69] A. D. Assefa, Y. S. Keum, and R. K. Saini, "A comprehensive study of polyphenols contents and antioxidant potential of 39 widely used spices and food condiments," *Journal of Food Measurement and Characterization*, vol. 12, no. 3, pp. 1548–1555, 2018.

[70] S. Xie, P. Huang, J. J. Kruzic, X. Zeng, and H. Qian, "A highly efficient degradation mechanism of methyl orange using Fe-based metallic glass powders," *Scientific Reports*, vol. 6, no. 1, p. 21947, 2016.

[71] C. C. Wang, J. R. Li, X. L. Lv, Y. Q. Zhang, and G. Guo, "Photocatalytic organic pollutants degradation in metal-organic frameworks," *Energy & Environmental Science*, vol. 7, no. 9, pp. 2831–2867, 2014.

[72] C. J. Knill and J. F. Kennedy, "CRC handbook of data on organic compounds," *Carbohydrate Polymers*, vol. 26, no. 3, p. 243, Jan. 1995.

[73] F. M. Arrazola-Dominguez, J. T. Ávila Salazar, C. G. Gomez Sierra, and S. Hernández Garrido, *Química orgánica experimental a escala semimicro y fundamentos de la espectroscopía*, Vol. 2, Instituto Politécnico Nacional, Mexico, 2016.

[74] E. Dutkova, M. Baláž, N. Daneu et al., "Properties of CuFeS2/TiO2 nanocomposite prepared by mechanochemical synthesis," *Materials*, vol. 15, no. 19, p. 6913, 2022.

[75] T. Ioannidou, M. Anagnostopoulou, D. Papoulis, K. C. Christoforidis, and I. A. Vasiliadou, "UiO-66/Palygorskite/TiO2 ternary composites as adsorbents and photocatalysts for methyl orange removal," *Applied Sciences*, vol. 12, no. 16, p. 8223, 2022.

[76] R. Chen, S. Ding, B. Wang, and X. Ren, "Preparation of ZnFe2O4@TiO2 novel core-shell photocatalyst by ultrasonic method and its photocatalytic degradation activity," *Coatings*, vol. 12, no. 10, p. 1407, 2022.

[77] W. Ko, B. J. Cha, Y. D. Kim, and H. O. Seo, "Sub-micro photocatalytic TiO2 particles for a water depollution: comparable removal efficiency to commercial P25 and easy separation via a simple sedimentation," *Catalysis Today*, vol. 403, no. 1, pp. 47–57, 2022.

[78] S. Palliyalil, R. K. V. Chola, S. Vigneshwaran, N. C. Poovathumkuzhi, B. M. Chelaveettil, and S. Meenakshi, "Ternary system of TiO2 confined chitosan–polyaniline heterostructure photocatalyst for the degradation of anionic and cationic dyes," *Environmental Technology and Innovation*, vol. 28, Article ID 102586, 2022.

[79] Y. Jin, W. Tang, J. Wang et al., "High photocatalytic activity of spent coffee grounds derived activated carbon-supported Ag/TiO2 catalyst for degradation of organic dyes and antibiotics," *Colloids and Surfaces A: Physicochemical and Engineering Aspects*, vol. 655, no. 5, Article ID 130316, 2022.

[80] H. Huang, S. Zhao, Y. Yang et al., "Axially wrinkled tubular SnO2/TiO2 heterostructures for effective degradation of organic pollutants," *Materials Science in Semiconductor Processing*, vol. 152, Article ID 107065, 2022.

[81] S. Ramasundaram, A. Balasankar, S. Arokiyaraj, P. Sumathi, and T. Hwan Oh, "Multi-useable titanium dioxide and poly(vinylidene fluoride) composite foam photocatalyst for degradation of organic pollutants," *Applied Surface Science*, vol. 609, no. 30, Article ID 155264, 2023.